Journal of
Radiation Protection and Research 2016;41(3):229-236
http://dx.doi.org/10.14407/jrpr.2016.41.3.229

pISSN 2508-1888 | eISSN 2466-2461

Fundamental Study of nanoDot OSL Dosimeters for Entrance Skin Dose Measurement in Diagnostic X-ray Examinations

Tohru Okazaki[1,*], Hiroaki Hayashi[2], Kazuki Takegami[2], Hiroki Okino[2], Natsumi Kimoto[2], Itsumi Maehata[2], Ikuo Kobayashi[1]

[1]Nagase Landauer, Ltd., Tsukuba; [2]Tokushima University, Tokushima, Japan

ABSTRACT

Background: In order to manage the patient exposure dose in X-ray diagnosis, it is preferred to evaluate the entrance skin dose; although there are some evaluations about entrance skin dose, a small number of report has been published for direct measurement of patient. We think that a small-type optically stimulated luminescence (OSL) dosimeter, named nanoDot, can achieve a direct measurement. For evaluations, the corrections of angular and energy dependences play an important role. In this study, we aimed to evaluate the angular and the energy dependences of nanoDot.

Materials and Methods: We used commercially available X-ray diagnostic equipment. For angular dependence measurement, a relative response of every 15 degrees of nanoDot was measured in 40-140 kV X-ray. And for energy dependence measurement, mono-energetic characteristic X-rays were generated using several materials by irradiating the diagnostic X-rays, and the nanoDot was irradiated by the characteristic X-rays. We evaluated the measured response in an energy range of 8.1-75.5 keV. In addition, we performed Monte-Carlo simulation to compare experimental results.

Results and Discussion: The experimental results were in good agreement with those of Monte-Carlo simulation. The angular dependence of nanoDot was almost steady with the response of 0 degrees except for 90 and 270 degrees. Furthermore, we found that difference of the response of nanoDot, where the nanoDot was irradiated from the randomly set directions, was estimated to be at most 5%. On the other hand, the response of nanoDot varies with the energy of incident X-rays; slightly increased to 20 keV and gradually decreased to 80 keV. These results are valuable to perform the precise evaluation of entrance skin dose with nanoDot in X-ray diagnosis.

Conclusion: The influence of angular dependence and energy dependence in X-ray diagnosis is not so large, and the nanoDot OSL dosimeter is considered to be suitable dosimeter for direct measurement of entrance surface dose of patient.

Keywords: OSL dosimeter, nanoDot, Angular dependence, Energy dependence, Diagnostic X-ray

Original Research

Received July 17, 2015
Revision March 28, 2016
Accepted May 27, 2016

Corresponding author: Tohru Okazaki

Nagase Landauer Ltd., C22-1 Suwa, Tsukuba, Ibaraki 300-2686, Japan
Tel: +81-298393304, Fax: +81-29-8368441
E-mail: okazaki@nagase-landauer.co.jp

Introduction

The exposure dose of patient has been increasing [1] caused by demand of the precise diagnosis, and exposure dose should be managed under consideration of quality of the medical images [2, 3]. To evaluate the patient dose in radiological examinations, it is prefer to measure exposed dose directly. Although some of dosimeters are used for

direct measurement in radiotherapy region [4-7], direct measurement in X-ray diagnosis is not performed because the most of dosimeters disturb medical images. Therefore an air-kerma measurement based on ionization chamber [8] with the consideration of a back scatter factor [9-13] is traditionally used for the evaluation of entrance skin dose in X-ray diagnosis.

In order to propose the patient dose management system, we focus on the ability of the optically stimulated luminescence (OSL) dosimeter [14-16]. The basic characteristics of the OSL dosimeter and its potential for clinical applications were reported elsewhere; procedure for high accuracy measurement [17], annealing equipment [18], energy dependence measurement [19], angular dependence [20, 21], comparison with thermoluminescence dosimeter [22], and applied measurement using anthropomorphic phantom [23]. Moreover, the OSL dosimeter's potential for the realistic clinical applications has been verified; the computed tomography [24, 25], interventional fluoroscopy [26] and so on. Combined with these studies, we proposed unique method [27, 28] for the conventional dose evaluation in which angular and/or energy dependences should not be considered. Figure 1 shows a demonstration of invisibility [29] using the small-type OSL dosimeter (nanoDot OSL dosimeter).The nanoDot OSL dosimeter can be achievable to perform the direct measurement of entrance skin dose in X-ray diagnosis. Although the basic characteristics of the nanoDot OSL dosimeter on diagnostic X-ray have been reported, the detailed properties are required to evaluate the entrance skin dose precisely.

The entrance skin dose is composed of primary X-ray and scattered X-rays. The amount of primary X-ray can be estimated by the condition of the irradiation, however that of scattered X-rays depends on the individual situation. In particular the distribution of the incidence direction and the energy of scattered X-rays vary with thickness of the subjects. For this reason, correcting the influence of the angular dependence and energy dependence of the dosimeter play an important role in direct measurement of entrance skin dose precisely. In this paper we studied the evaluation of angular dependence and energy dependence of the nanoDot OSL dosimeter in diagnostic X-ray region.

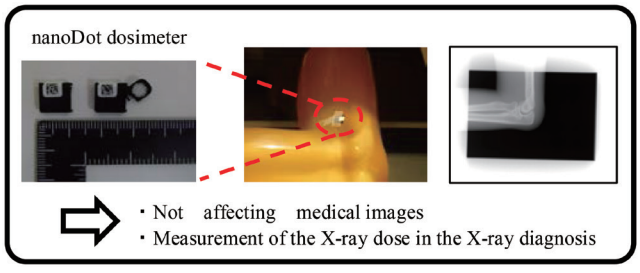

Fig. 1. 10 mm×10 mm×2 mm of nanoDot optically stimulated luminescence (OSL) dosimeter does not affect a medical image. It is achievable of direct measurement of entrance skin dose in X-ray diagnosis.

Materials and Methods

1. Materials

A commercialized X-ray apparatus (MRAD-A 50S/70, TOSHIBA medical systems corp., Otawara, Japan) was used for the experiment. The original collimator [30] was used to reduce the scattered X-ray from removable diaphragm and confine the primary X-ray beam to the size of exposed sample.

The dose data of OSL dosimeter can be initialized by visible light annealing process [16, 18]. The nanoDot OSL dosimeters, annealed well by original equipment [18], were used for the experiments. Irradiated nanoDot OSL dosimeters were read out consecutive 5 times by microStar and the sensitivity corrected counts were used for the evaluation of angular dependence and energy dependence. The uncertainty of the measurements was estimated based on the previous report [17].

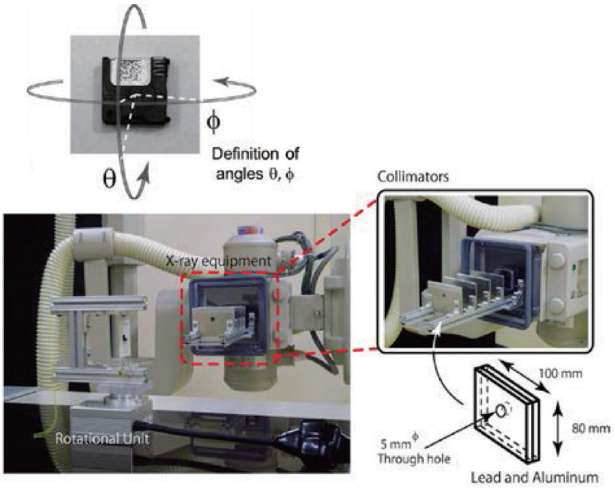

Fig. 2. The experimental setup of angular dependence measurement. The primary X-ray generated by clinical X-ray apparatus was collimated by original equipment. A nanoDot OSL dosimeter was irradiated with collimated X-ray beam without scattering radiations. The nanoDot OSL dosimeter was rotated to two different direction θ and φ.

http://dx.doi.org/10.14407/jrpr.2016.41.3.229

2. Experiment

Figure 2 shows the experimental setup of angular dependence experiment. A nanoDot OSL dosimeter was attached on a thin film (Parafilm™, Pechiney Plastic Packing Company, Chicago, USA) and fixed to a remotely-controlled rotational unit. Source to dosimeter distance was 1.5 m. A nanoDot OSL dosimeter was rotated on two different axes; θ and φ defined in Figure 2 40-140 kV of X-rays were collimated to be 2 cm-radius and were irradiated to a dosimeter which was set in air condition. The angle of irradiation was rotated to every 15 degrees.

Figure 3 shows the experimental setup of energy dependence experiment. The characteristic X-ray source material was put into micro test tube and set to the center of the setup. Then, it was exposed by a 5 mm-radius collimated primary X-ray. A nanoDot OSL dosimeter was set to be 1 cm distance from the micro test tube in perpendicular direction of primary X-ray. To reduce influence of the scattered X-ray, the dosimeter was shielded by 2 mm thickness of lead plate. On the opposite side of the sample material, CdTe semiconductor detector (123-0 type, EMF Japan Co., Osaka, Japan) was set in 5 cm distance from the sample to determine energy fluence and/or air kerma of the characteristic X-rays. To reduce the influence of scattered X-ray, the detector was also shielded. The characteristic X-ray source materials are listed in Table 1. The elemental substances, oxidized, or carbonate samples were used for the characteristic X-ray source materials because the energies of characteristic X-ray generated by oxygen and carbon were negligibly low. The weighted mean energy of K_α and K_β X-rays, effective energy, was used for the analysis. The energy range of characteristic X-rays was 8.1-75.5 keV.

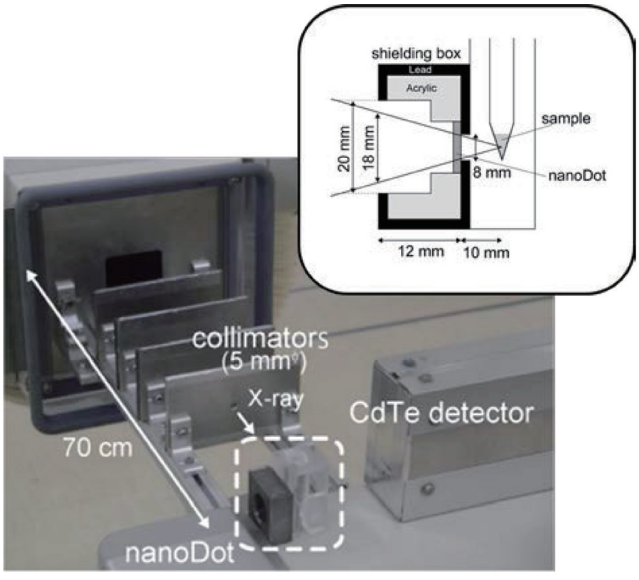

Fig. 3. The experimental setup of energy dependence measurement. A nanoDot OSL dosimeter and a CdTe detector were set on the opposite side of characteristic X-ray source in perpendicular to direction of primary X-ray. The nanoDot OSL dosimeter was shielded to reduce scattered X-rays. To minimize the influence of scattered X-ray, the size of aperture and way out of the shield was designed.

When the primary X-ray was irradiated, not only the characteristic X-ray but also Compton scattered X-rays were generated. For estimating the contribution of the Compton scattered X-rays, water sample was irradiated and the contribution of them were subtracted from the sample of interest. Then, the spectra of characteristic X-rays used for the irradiation of the nanoDot OSL dosimeter were derived by the spectra measured with the CdTe detector; using the Monte Carlo simulation code [31], response functions of the CdTe detector were calculated [32] and the measured spectra were unfolded. Here, the air kerma corresponding to the characteristic X-rays was calculated by the unfolded spectrum and the mass energy absorption coefficient [33]. At the cases of Au and Pb samples irradiation, LX-rays were emitted in addition to the KX-rays. The contribution of LX-rays was subtracted based on the simulated energy dependence of nanoDot OSL dosimeter as described in the next section.

3. Monte Carlo Simulation

To evaluate the experimental results, Monte Carlo simulation (EGS5: electron gamma shower ver. 5) [31] was per-

Table 1. Properties of the Prepared Metallic Samples, Energies and Air Kerma of the Characteristic X-rays

Samples (Atomic number: Composition)	Effective energy of characteristic X-rays [keV]	Air kerma estimated by the response of CdTe detector [mGy]
29: Cu	8.1	0.09±0.01
39: Y_2O_3	15.2	0.33±0.01
41: Nb_2O_3	16.9	0.43±0.01
47: Ag	22.6	0.15±0.01
49: In	24.7	0.21±0.01
50: SnO_2	25.8	0.19±0.01
55: Cs_2CO_3	31.6	1.00±0.02
56: $BaCO_3$	32.9	1.36±0.03
57: La_2O_3	34.1	1.32±0.03
63: Eu_2O_3	42.4	1.16±0.03
64: Gd_2O_3	43.9	1.09±0.03
74: WO_3	60.6	0.59±0.02
79: Au	70.3	0.52±0.02
82: Pb	75.5	0.42±0.01

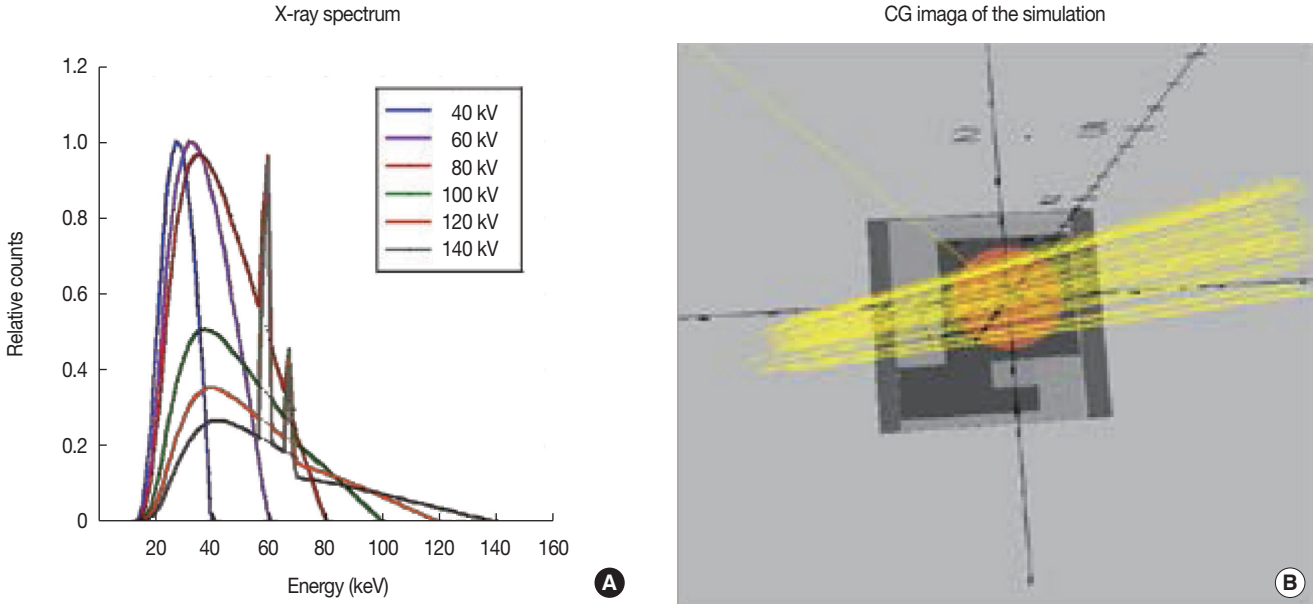

Fig. 4. The concept of Monte Carlo simulation. (A) shows the X-ray spectra generated from the clinical X-ray apparatus. Even if the tube voltage varies, the mean energy of the X-rays is within 30-40 keV. (B) shows the CG image of Monte Carlo simulation. For an efficient simulation, the X-rays were just introduced to the detection region of the nanoDot OSL dosimeter.

formed. For construction of nanoDot in the simulation, micro-CT images assessed by Lehmann et al. [20] were used. For the calculation of energy dependence, mono-energetic X-rays were introduced to the nanoDot OSL dosimeter. For the angular dependence, X-ray spectra were introduced. Moreover, the following simulations were performed; 1) simulations without plastic case for evaluating the absorptions of X-rays in the plastic case of the nanoDot OSL dosimeter, and 2) randomly irradiation to evaluate the clinically using situation. The spectra of primary X-rays estimated by Birch's formula [34] were applied as shown in Figure 4A. Figure 4B shows computer graphic image of the simulation. For an efficient simulation, the X-rays were just introduced to the detection region of the nanoDot OSL dosimeter.

Results and Discussion

1. Angular Dependence

Figures 5 and 6 show the comparison of experimental and simulated angular dependences for θ and φ directions, respectively. Solid circles show experimental data, and dashed lines show simulated ones. The experimental data were in good agreement with the simulation.

We discuss the cause of the response decreasing in 90 degrees and 270 degrees. We estimate the influence of the absorption by the construction of dosimeter and OSL material itself. Figure 7 is the simulated results of angular dependence in 40 kV X-ray between with and without the case. The effect of the geometric efficiency (solid angle) is 20% and the self-absorption of the construction is 5%. In higher energy X-rays than 40 kV, the absorption rate becomes smaller, because the attenuation rate of 40 kV is much higher than that of the others. Therefore, the above mentioned absorption rate is considered to be maximum in diagnostic X-rays.

To evaluate the entrance skin dose precisely, the angular dependence correction of nanoDot OSL dosimeter with the estimated incident X-ray spectrum is effective. However, it is difficult to estimate the incident X-ray because the scattered X-ray varies with the irradiation condition and the figure of the patient. Accordingly, we estimated the influence of angular dependence with a simple model using the Monte-Carlo simulation. Figure 8 shows the comparison of the responses in 0 degrees irradiation and the 4π random irradiation. The reduction of responses in randomly irradiation by 4 π directions is less than 4% in energy range of 40-140 kV.

2. Energy Dependence

The air kerma corresponding the characteristic X-rays "K" was estimated by the response of CdTe detector based on the following formula [8]:

$$K = \int (F_S(E) - F_W(E) \times CF) \times E \times ((\mu_{en}(E))/\rho)_{air}\, dE. \quad (1)$$

http://dx.doi.org/10.14407/jrpr.2016.41.3.229

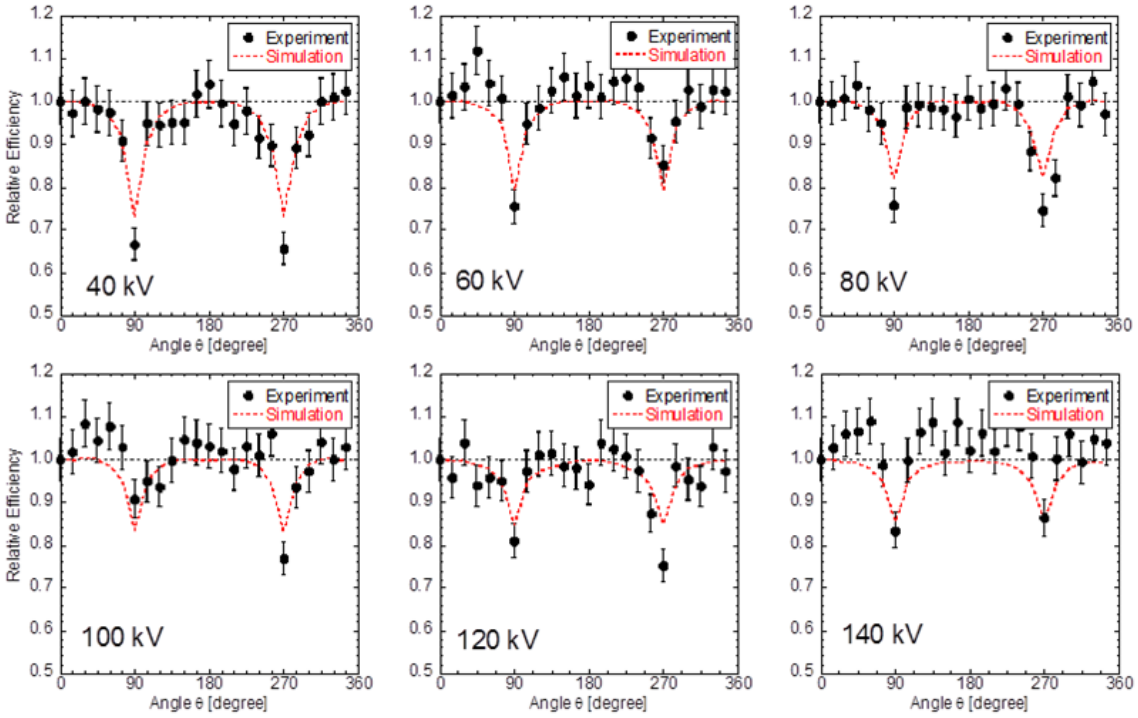

Fig. 5. The comparison between experimental and simulated data in theta direction of rotation. The experimental data are in good agreement with the simulation. The response of nanoDot OSL dosimeter decreases in 90 and 270 degrees, and the tendency is noticeable in low energy X-rays.

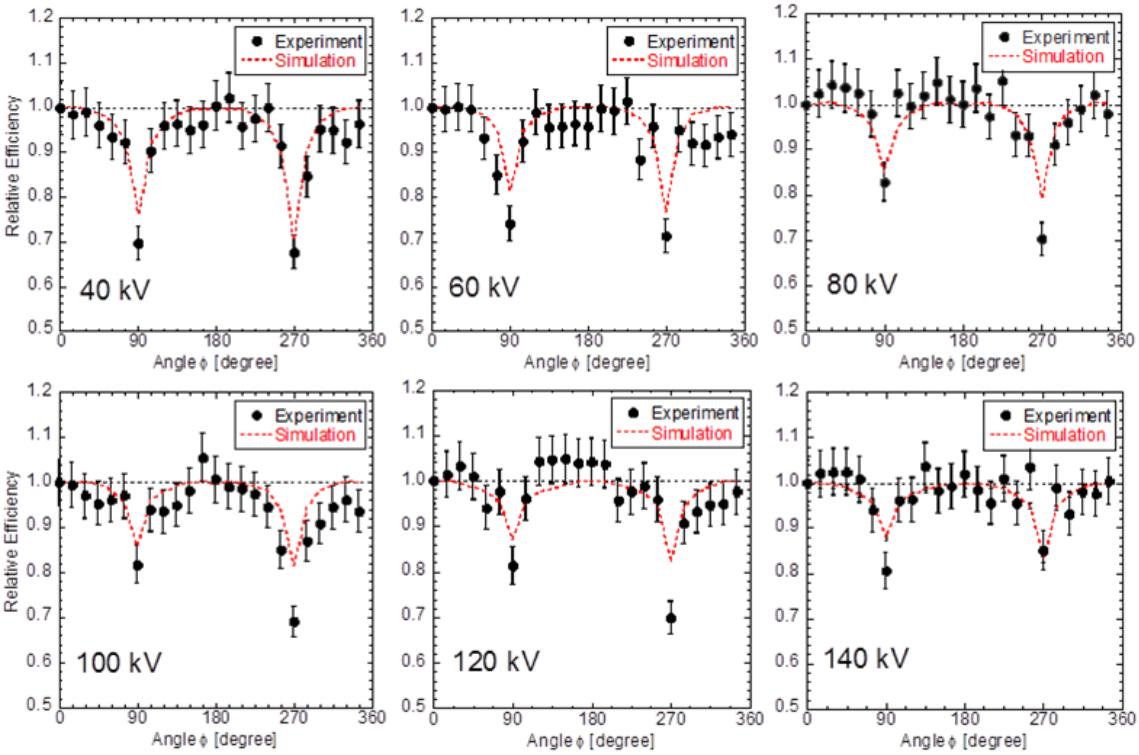

Fig. 6. The comparison between experimental and simulated data in phi direction of rotation. The experimental data of phi direction are also in good agreement with the simulation.

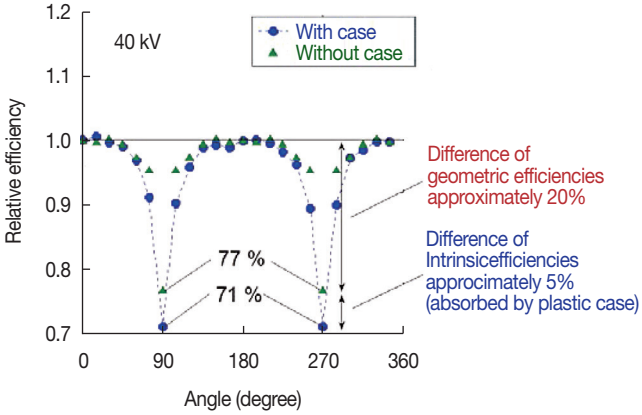

Fig. 7. Estimation of the cause of the response decreasing in 90 and 270 degrees by Monte Carlo simulation. As the result of comparison, the attenuation rate with/without the case differs approximately 5%. Accordingly, the remaining 20% of attenuation comes from the effect of the reduction of solid angle.

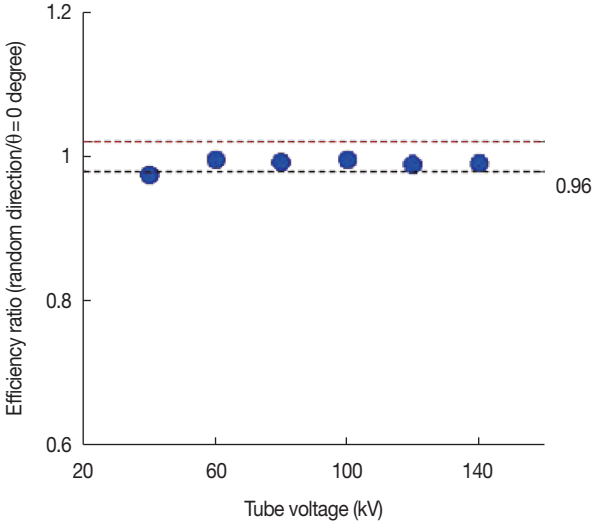

Fig. 8. Estimation of the effect of the angular dependence, compared the simulated response of nanoDot OSL dosimeter between 0 degrees irradiation and 4 pi irradiation in 40-140 kV X-rays. Although the ratio of 40 kV is the lowest, it even keeps 0.96.

F_S (E): The number of energy E photon in the source material irradiation

F_W (E): The number of energy E BG photon evaluatedby H_2O sample irradiation

CF: Correction factor of the BG photon contribution rate in the source material irradiation

$(\mu_{en}(E)/\rho)_{air}$: mass energy absorption coefficient of the air

The air kerma obtained in this study is presented in Table 1. They were determined with accuracy of 2-8%. The nanoDot OSL dosimeters were also exposed by characteristic X-ray and/or background (BG) X-ray. In the same manner as CdTe detector, the contribution from BG in measured counts of the dosimeter was subtracted using the same correction factor; CF. The energy dependence data was defined as the ratio of response of nanoDot divided by the air kerma evaluated by the CdTe detector. The result of energy dependence normalized at 30 keV was shown in Figure 9 and these data were also summarized in Table 2. The experimental data were in good agreement with the simulated ones. In the Figure 9, the

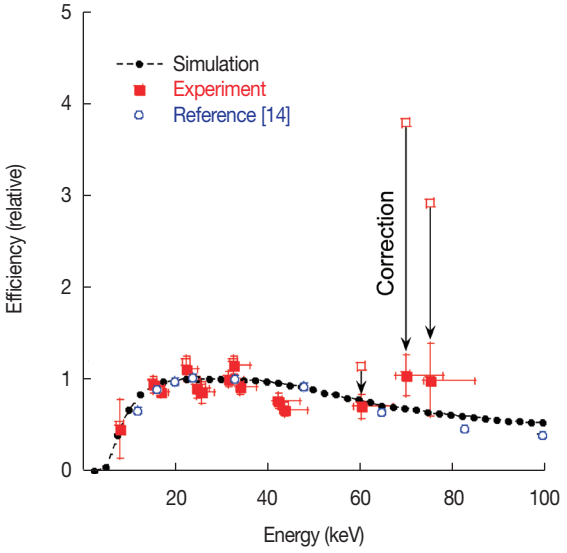

Fig. 9. The comparison of energy dependence in 8.1–75.5 keV between experimental and simulated data. In the characteristic X-ray of Au and Pb, the responses of nanoDot OSL dosimeter were corrected accordingly the responses of them include LX-rays as well as KX-rays. The experimental data are in good agreement with the simulation.

Table 2. Energy Dependence of the nanoDot OSL Dosimeter Measured with the Current Experiment

Average energy [keV]	Relative responses
8.1	0.46 ± 0.32
15.2	0.94 ± 0.09
16.9	0.87 ± 0.05
22.6	1.12 ± 0.14
24.7	0.91 ± 0.12
25.8	0.86 ± 0.12
31.6	1.00 ± 0.08
32.9	1.15 ± 0.10
34.1	0.92 ± 0.08
42.4	0.76 ± 0.09
43.9	0.67 ± 0.07
60.6	0.71 ± 0.13
70.3	1.04 ± 0.22
75.5	0.99 ± 0.40

http://dx.doi.org/10.14407/jrpr.2016.41.3.229

precisely determined experimental values reported by Eduardo et al. [14] were also plotted. Their data were determined using the standardized X-rays, and it was clarified that our data was consistent with their data. The response of nanoDot OSL dosimeter varies with the energy and the difference is double at a maximum between 8.1 keV and 30 keV. However, it has little chance for the nanoDot OSL dosimeter to be exposed by 8 keV and 30 keV X-rays simultaneously in X-ray diagnosis. When the direct measurement of entrance skin dose is performed, the nanoDot is mainly exposed by primary X-ray and Compton scattered X-rays which are emitted from the body of the patient. In this situation, the energy of Compton scattered X-ray generated by 30 keV of primary X-ray is at most 26 keV. Namely, the difference of the energy is only 4 keV and the influence of the energy dependence of nanoDot OSL dosimeter is less than 1%. That is negligibly small.

Conclusion

The nanoDot OSL dosimeter, does not disturb the medical image, is useful tool for direct measurement of patient dose in X-ray diagnosis. To evaluate the entrance skin dose with the dosimeter precisely, the correction of angular dependence and energy dependence based on the experiment and simulation is preferred. Hence we measured the angular dependence and energy dependence of nanoDot in the energy range of diagnosis. The simulated results were in good agreement with the experiments. Moreover, we estimate the influence of angular dependence and energy dependence with simple model. In conclusion, we evaluated that the entrance skin dose can be measured by the nanoDot OSL dosimeter with only 5% of deviation. For clinical application, more precise experiment and analysis are now in progress.

References

1. Gonzalez AB, Darby S, Risk of cancer from diagnostic X-ray: estimates for the UK and 14 other countries. Lancet. 2004;363:345-351.
2. Uffmann M, Prokop CS, Digital radiography: the balance between image quality and required radiation dose. Eur. J. Radiol. 2009;72:202-208.
3. Gardner SJ, Studenski MT, Giaddui T, Cui Y, Galvin J, Yu Y, Xiao Y. Investigation into image quality and dose for different patient geometries with multiple cone-beam CT systems. Med. Phys. 2014; 41(3):031908-1-11.
4. American Association of Physicists in Medicine by the American Institute of Physics. Fetal dose from radiotherapy with photon beams. AAPM Report No.50. 1995; 63-82.
5. Piesch E, Burgkhardt B, Vilgis M, Photoluminescence dosimetry: progress and present state of art. Radiat. Prot. Dosim.1990; 33:215-226.
6. Cho SJ, Kim WT, Ki YG, Kwon SI, Lee SH, Huh DH, Cho KH, Kwon BH, Kim DW. In vivo dosimetry with MOSFET detector during radiotherapy. World congress on medical physics and biomedical engineering. Seoul, Korea. August 27 – September 1, 2006.
7. Bao Q, Hrycushko BA, Dugas JP, Hager FH, Solberg TD. A technique for pediatric total skin electron irradiation. Radiat. Oncol. 2012; 7(40):1-7.
8. Maehata I, Hayashi H, Kimoto N, Takegami K, Okino H, Kanazawa Y, Tominaga M. Practical method for determination of air kerma by use of an ionization chamber toward construction of a secondary X-ray field to be used in clinical examination rooms. Radiol. Phys. Tech. 2016; 9(2):193-201.
9. Grosswendt B, Backscatter factors for x-rays generated at voltages between 10 and 100 keV. Phys. Med. Biol. 1984; 29(5):579-591.
10. Klevenhagen SC. Experimentally determined backscatter factors for x-rays generated at voltages between 16 and 140 kV. Phys. Med. Biol. 1989; 34(12):1871-1882.
11. Grosswendt B. Dependences of the photon backscatter factor for water on source-to-phantom distance and irradiation field size. Phys. Med. Biol. 1990; 35(9):1233-1245.
12. Kato H. Method of calculating the backscatter factor for diagnostic x-rays using the differential backscatter factor. Jpn. J. Radiol. Technol. 2001; 57(12):1503-1510.
13. Kato H, Minami K, Asada Y, Suzuki S. Analysis of scattered radiation in an irradiated body by means of the monte carlo simulation: Back-scatter factors of diagnostic x-rays in the incident surface which is not flat. Jpn. J. Radiol. Technol. 2016; 72(5):396-401.
14. Yukihara EG, McKeever SWS. Optically stimulated luminescence fundamentals and applications. 1st Ed. Chichester, UK. John Wiley &Sons, Inc. 2011;129-140.
15. Pradhan AS, Lee JI, Kim JL. Recent developments of optically stimulated luminescence materials and techniques for radiation dosimetry and clinical applications. Journal of Medical Physics. 2008;33(3):85-99.
16. Jursinic PA. Characterization of optically stimulated luminescent dosimeters, OSLDs, for clinical dosimetric measurements. Med. Phys. 2007;34(12):4594-4604.
17. Hayashi H, Nakagawa K, Okino H, Takegami K, Okazaki T, Kobayashi I. High accuracy measurements by consecutive readings of OSL dosimeter. Medical Imaging and Information Sciences. 2014;31(2):28-34.
18. Nakagawa K, Hayashi H, Okino H, Takegami K, Okazaki T, Ko-

bayashi I. Fabrication of annealing equipment for optically stimulated luminescence (OSL) Dosimeter. Jpn. J. Radiol. Technol. 2014;70(10):1135-1142.
19. Reft CS. The energy dependence and dose response of a commercial optically stimulated luminescent detector for kilovoltage photon, megavoltage photon, and electron, proton, and carbon beams. Med. Phys. 2009;36(5):1690-1699.
20. Lehmann J, Dunn L, Lye JE, Kenny JW, Alves AD, Cole A, Asena A, Kron T, Williams IM. Angular dependence of the response of the nanoDot OSLD system for measurements at depth in clinical megavoltage beams. Med. Phys. 2014;41(6):061712-1-9.
21. Al-Senan RM, Hatab MR. Characteristics of an OSLD in the diagnostic energy range. Med. Phys. 2011;38(7):4396-4405.
22. Valiyaparambil JV, Mallya SM. Characterization of an optically stimulated dosimeter for dentomaxillofacial dosimetry. Oral. Surg. Oral. Med. Oral. Pathol. Oral. Radiol. Endod. 2011;112 (6):793-797.
23. Endo A, Katoh T, Kobayashi I, Joshi R, Sur J, Okano T. Characterization of optically stimulated luminescence dosemeters to measure organ doses in diagnostic radiology. Dentomaxillofac. Rad. 2012;41(3):211-216.
24. Endo A, Katoh T, Vasudeva SB, Kobayashi I, Okano T. A preliminary study to determine the diagnostic reference level using dose-area product for limited-area cone beam CT. Dentomaxillofac. Rad. 2013;42(4):20120097-1-6.
25. Yukihara EG, Ruan C, Gasparian PBR, Clouse WJ, Kalavagunta C, Ahmad S. An optically stimulated luminescence system to measure dose profiles in x-ray computed tomography. Phys. Med. Biol. 2009;54(20):6337-6352.
26. Gaspariian PBR, Ruan C, Ahmad S, Kalavagunta C, Cheng CY, Yukihara EG. Demonstrating the use of optically stimulated luminescence dosimeters (OSLDs) for measurement of staff radiation exposure in interventional fluoroscopy and helmet output factors in radiosurgery. Radiat. Meas. 2010;45:677-680.
27. Takegami K, Hayashi H, Nakagawa K, Okino H, Okazaki T, Kobayashi I. Measurement method of an exposed dose using the nanoDot dosimeter (EPOS). EPOS of European Congress of Radiology. Vienna, Austria. Mar. 4-8, 2015.
28. Takegami K, Hayashi H, Okino H, Kimoto N, Maehata I, Kanazawa Y, Okazaki T, Kobayashi I. Practical calibration curve of small-type optically stimulated luminescence (OSL) dosimeter for evaluation of entrance-skin dose in the diagnostic X-ray. Radiol. Phys. Technol. 2015;8(2):286-294.
29. Takegami K, Hayashi H, Okino H, Kimoto N, Maehata I, Kanazawa Y, Okazaki T, Hashizume T, Kobayashi I. Estimation of identification limit for a small-type OSL dosimeter on the medical images by measurement of X-ray spectra. Radiol. Phys. Technol. 2016;9(2):286-292.
30. Takegami K, Hayashi H, Konishi Y, Fukuda I. Development of multistage collimator for narrow beam production using filter guides of diagnostic X-ray equipment and improvement of apparatuses for practical training. Med. Imaging Inf. Sci. 2013; 30(4):101-107.
31. Hirayama H, Namito Y, Bielajew AF, Wilderman SJ, Nelson WR. The EGS5 code system. KEK Report 2005-8. 2005;1-441.
32. Okino H, Hayashi H, Nakagawa K, Takegami K. Measurement of response function of CdTe detector using diagnostic x-ray equipment and evaluation of monte carlo simulation code. Jpn. J. Radiol. Technol. 2014;70(12):1381-1391.
33. Hubbell JH, Photon mass attenuation and energy-absorption coefficients. The International J. Appl. Radiat. Isot. 1982; 33(11): 1269-90.
34. Birch R, Marshall M. Computation of bremsstrahlung X-ray spectra and comparison with spectra measured with a Ge(Li) detector. Phys. Med. Biol. 1979;29(3):505-517.

 http://dx.doi.org/10.14407/jrpr.2016.41.3.229